Dual Orbital Degeneracy Lifting in a Strongly Correlated Electron System

R. J. Koch,[1,*] R. Sinclair,[2] M. T. McDonnell,[3,†] R. Yu,[1,‡] M. Abeykoon,[4] M. G. Tucker,[3] A. M. Tsvelik,[1] S. J. L. Billinge,[1,5] H. D. Zhou,[2] W.-G. Yin,[1,§] and E. S. Bozin[1,‖]

[1]*Condensed Matter Physics and Materials Science Division, Brookhaven National Laboratory, Upton, New York 11973, USA*
[2]*Department of Physics and Astronomy, University of Tennessee, Knoxville, Tennessee 37996, USA*
[3]*Neutron Scattering Division, Oak Ridge National Laboratory, Oak Ridge, Tennessee 37831, USA*
[4]*Photon Sciences Division, Brookhaven National Laboratory, Upton, New York 11973, USA*
[5]*Department of Applied Physics and Applied Mathematics, Columbia University, New York, New York 10027, USA*

(Received 29 September 2020; accepted 29 March 2021; published 6 May 2021)

The local structure of $NaTiSi_2O_6$ is examined across its Ti-dimerization orbital-assisted Peierls transition at 210 K. An atomic pair distribution function approach evidences local symmetry breaking preexisting far above the transition. The analysis unravels that, on warming, the dimers evolve into a short range orbital degeneracy lifted (ODL) state of dual orbital character, persisting up to at least 490 K. The ODL state is correlated over the length scale spanning ~6 sites of the Ti zigzag chains. Results imply that the ODL phenomenology extends to strongly correlated electron systems.

DOI: 10.1103/PhysRevLett.126.186402

Introduction.—The emergence of technologically relevant quantum orders in materials [1] stems from complex interaction of electronic charge, spin, and orbitals and their coupling to the host lattice [2,3]. Orbital sector is often engaged in transition metal systems, owing to partially filled d manifolds [4]. Because of the coupling to both spin and lattice, of particular interest is when the lattice topology imposes orbital degeneracy [5] and/or electronic frustration [6]. The removal of orbital degeneracy and the relief of frustration impact symmetry lowering and electronic properties [7]. Complexities of the low temperature symmetry breaking have been thoroughly studied in relation to diverse emergent behaviors such as frustrated magnetism [8,9], colossal magnetoresistivity [10], charge and orbital order [11,12], metal-insulator transition [13–15], pseudogap [16,17], and high temperature superconductivity [18,19]. Their understanding employs Fermi surface nesting [20,21], Peierls [22,23], and band Jahn-Teller mechanisms [24,25].

When orbital degeneracies are anticipated, it is often assumed that crystallographic symmetry lowering at the temperature driven phase transitions implies simultaneous orbital degeneracy lifting (ODL) via some cooperative mechanism [5,6,26]. Consequently, the high temperature regimes possessing high crystallographic symmetry remain less explored. In contrast, probes of local symmetry qualify the ODL as a local electronic effect existing at temperatures well above [27,28] the global symmetry breaking transitions. In spinels $CuIr_2S_4$ [27] and $MgTi_2O_4$ [28] with weak electron correlations, a highly localized ODL state involving two transition metal ions is discovered as a high-temperature precursor to an orbitally driven metal-insulator transition [29]. Albeit discontinuously connected to the ground state, the ODL in these spinels is a prerequisite for charge and orbital order and spin dimerization [11,30,31], thus, enabling the transition.

The ubiquity and role of the ODL in the emergent phenomena are yet to be established [28,32]. It is important to understand whether the ODL state is a peculiarity of weakly coupled electronic systems in proximity to a localized-to-itinerant crossover, or if it could also be realized deep in the Mott insulating regime with strong on-site Coulomb interactions, where the charge fluctuations are suppressed. An opportunity to explore this is offered by the quasi-one-dimensional $NaTiSi_2O_6$ clinopyroxene [33], one of the rock-forming silicate minerals constituting the upper Earth's mantle [34]. It is a paramagnetic strongly correlated Mott insulator with a ~2 eV gap [35], featuring zigzag chains of skew edge-shared TiO_6 [Figs. 1(a) and 1(b)], with Ti^{3+} in d^1 ($S = 1/2$) nominally triply degenerate t_{2g} orbital configuration. The ground state of $NaTiSi_2O_6$ with a 53 meV spin gap [36] establishes on cooling through a 210 K [37] structural transition where ferro-orbital ordering stabilizes intrachain Ti spin singlet dimerization [38]. Once thought to host Haldane $S = 1$ chains [35,39,40], $NaTiSi_2O_6$ is considered a candidate for quantum liquid with strong orbital fluctuations [41].

By combining neutron and x-ray total scattering based atomic pair distribution function (NPDF and XPDF) approaches [42], we find compelling local structural evidence for a fluctuating ODL state of dual orbital character in $NaTiSi_2O_6$ at high temperature. The spatial extent of associated short range structural correlations consistent with Peierls-like instability at $1/6$ filling suggests relevance of all three Ti t_{2g} orbitals in this regime. The pair distribution function (PDF) observations establish that

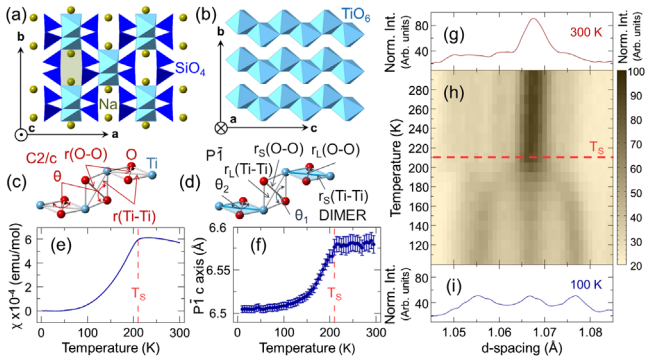

FIG. 1. Properties of $NaTiSi_2O_6$. (a) $C2/c$ structure; (b) quasi-1D zigzag TiO_6 chains; (c) undistorted TiO_2 plaquettes of the $C2/c$ phase featuring uniform Ti-Ti and O-O distances; (d) distorted TiO_2 plaquettes of the dimerized $P\bar{1}$ phase with Ti-Ti and O-O distances bifurcated (S = short, L = long); (e) the Curie law subtracted dc magnetic susceptibility; (f) the c axis parameter from $P\bar{1}$ model fits to the XPDF data; (g)–(i) temperature evolution of a selected segment of neutron total scattering data. Note: zigzag chains run along c axis in $C2/c$, and along a axis in $P\bar{1}$.

the ODL phenomenology does extend to materials with strong electron correlations, reinforcing the notion of its ubiquity. This intricate short range orbital precursor to spin dimerization provides a rationale for a number of puzzling high temperature anomalies reported for this system [36,43,44].

Polycrystalline $NaTiSi_2O_6$ used in powder diffraction measurements was obtained via a solid state route [36,37,45] and displays a transition to a spin-singlet dimer state at $T_s = 210$ K, Fig. 1(e). Total scattering data for PDF analysis were collected over 100 K $\leq T \leq$ 300 K (neutrons), and over 10 K $\leq T \leq$ 300 K range and at 490 K (x rays). The approach utilizes both Bragg and diffuse scattering, and provides information on the average structure and on the local deviations from it [42]. Robust crystallographic symmetry change at T_s is evident in the x ray [Fig. 1(f)], and neutron data [Figs. 1(g)–1(i)]. Experimental and analysis details are provided in the Supplemental Material [45].

Crystallographic perspective.—$NaTiSi_2O_6$ crystallizes in a monoclinic $C2/c$ structure, Fig. 1(a), featuring characteristic zigzag chains of edge-sharing TiO_6 octahedra, Fig. 1(b), giving the system a quasi-one-dimensional character [38]. The chains are embedded in a somewhat disordered SiO_4 network encompassing Na [45,54,55]. Within the chains, the shared-edge O pairs and Ti centers constitute TiO_2 plaquettes, identical in $C2/c$, which alternate in orientation, as shown in Fig. 1(c). Magnetically active Ti have +3 valence in $3d^1$ configuration [56], confirmed by neutron Rietveld refinement based bond valence sum calculations [45,57]. The dominant octahedral crystal field splits the Ti $3d$ orbitals into a partially filled t_{2g} triplet and an empty e_g doublet [37]. Nominally triply degenerate t_{2g} orbitals [5] are oriented toward the TiO_6 edges: xy and zx point toward the common edges of the zigzag chains, while yz is perpendicular to the general chain direction (for illustration see the top right corner inset in Fig. 5). Partial degeneracy alleviation is expected from slight trigonal distortion of TiO_6 [43], placing the single electron into a two fold degenerate low lying t_{2g}-derived (zx, xy) doublet [41] and rendering the third (yz) orbital inert [36,43,58]. The edge-sharing topology fosters direct (xy, xy) and (zx, zx) overlaps of t_{2g} orbitals belonging to neighboring Ti along the chains. This promotes Ti-Ti dimerization [43] in the ferro-orbitally ordered regime [38] upon cooling below T_s, lifting the t_{2g} degeneracy and lowering the average symmetry to triclinic ($P\bar{1}$) [56].

The average structure change observed in diffraction across the transition is associated with the splitting of Ti-Ti distances in the zigzag chains. The dimerization takes place within the TiO_2 plaquettes of just one of the two available orientations [zig or zag, Fig. 5(b)]. Consequentially, the Ti-Ti and O-O interatomic distances on the plaquettes bifurcate, Fig. 1(d): Ti-Ti (3.18 Å) and O-O (2.74 Å) contacts on the plaquettes in $C2/c$ become (3.11 Å, 3.22 Å) and (2.69 Å, 2.81 Å) in $P\bar{1}$, respectively. The dimerized plaquette has nominally two electrons ($2e$) [56] [see Fig. 5(a)]. Neighboring TiO_2 plaquettes become inequivalent as the Ti dimers and the associated $\cdots - 2e - 0e - 2e - 0e - \cdots$ bond-charge order form, thus, removing the zx-xy degeneracy. The $C2/c$ and $P\bar{1}$ models explain our neutron Bragg data in the high and low temperature regimes, respectively [45]. All Ti sites participate in dimerization in $P\bar{1}$ but remain equivalent (+3 valence) [45,56]. The fingerprint of the average structural change across T_s, simulated using crystallographic models [56] for NPDF [Figs. 2(a) and 2(b)] and XPDF [Figs. 2(c) and 2(d)], illustrates the expected PDF response should the local structure follow the average behavior. In Figs. 2(c) and 2(f), the crystallographically observed Ti-Ti splitting [56] is shown by scattering-weighted partial PDFs, revealing a

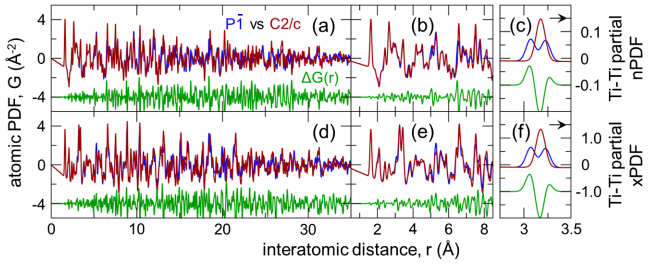

FIG. 2. Comparison of simulated PDFs. Crystallographic $P\bar{1}$ (blue) and $C2/c$ (red) models with their differential (green) offset for clarity for neutron probe over a wide (a) and a narrow (b) r range. (c) Neutron Ti-Ti partial PDF for the two models. Corresponding PDFs for x-ray probe are shown in (d)–(f). Simulations use uniform 0.001 Å^2 atomic displacement parameters for all atoms, and are scaled to match the data shown in Fig. 3.

considerably weaker signal in NPDF than in XPDF case. The pair contributions to PDF of Ti-Ti when compared to O-O are an order of magnitude stronger in XPDF, whereas in NPDF, they are three times weaker.

Local perspective.—While crystallography implies that the lifting of Ti orbital degeneracy and associated dimer formation occur at T_s, the complexity increases when the local structure information from PDF data is considered. If we compare the PDF signal from $T = 150$ K (well below T_s) to that from $T = 230$ K (just above T_s), the difference signal ΔG for interatomic distances $r > 15$ Å is large, as expected when passing through a structural transition [Figs. 3(a) and 3(c)]. However, and in contrast to the expectations shown in Fig. 2, ΔG is substantially smaller over the shorter distances ($r < 15$ Å) reflecting local structure, as highlighted in Figs. 3(e) and 3(g), especially in the NPDF case, which is less sensitive to Ti.

Actually, the local ΔG observed across the transition is comparable in magnitude to that observed in a 70 K difference ΔG which is fully above the transition [Figs. 3(e)–3(h)], where only changes due to thermal motion variations are expected. While the structural transition associated with the dimer formation is clearly apparent in the average structure, the same cannot be said regarding the local structure, revealing a curious local vs average disparity in $NaTiSi_2O_6$. This may suggest that spin singlet dimers do not disassemble locally on warming across T_s, in contrast to magnetic susceptibility measurements according to which the spin singlet dimers cannot be retained above the transition. We argue that the transition is not of a trivial order-disorder type, as one may deduce from the NPDF analysis alone [45], Figs. 3(a) and 3(b), but that it has an ODL-type character [27] evident from the XPDF analysis. In contrast to the differential NPDF signal implying minute change across the transition over the length scale corresponding to ~6 Ti sites, the ΔG signal in XPDF, Figs. 3(c) and 3(d), suggests that some local structural modification does occur at T_s.

Vanishing spin singlets.—This motivates a closer look at the temperature resolved XPDF data. Temperature evolution of the PDF differential, $\Delta G(T)$, underneath the Ti-Ti PDF peak at ~3.2 Å, where the dimer signal should be present, is particularly informative. Comparing the data at $T = 90$ K ($T < T_s$) and at T_s reveals a subtle but clear shift in pair probability from shorter to longer distances, Fig. 4(a), with an "M" shaped feature in $\Delta G(T)$, consistent with removal of the dimer distortion. When data at T_s and at $T = 300$ K ($T > T_s$) are compared, Fig. 4(b), the differential is much smaller for a comparable temperature difference. The NPDF data are not sensitive to this not only due to unfavorable scattering contrast, but also because the dimer-related distortions involve Ti and O displacements of opposite sign on the TiO_2 plaquettes, Fig. 5(a). For systematic assessment, we use a high temperature reference for calculating $\Delta G(T)$ [45]. The evolution of the $\Delta G(T)$

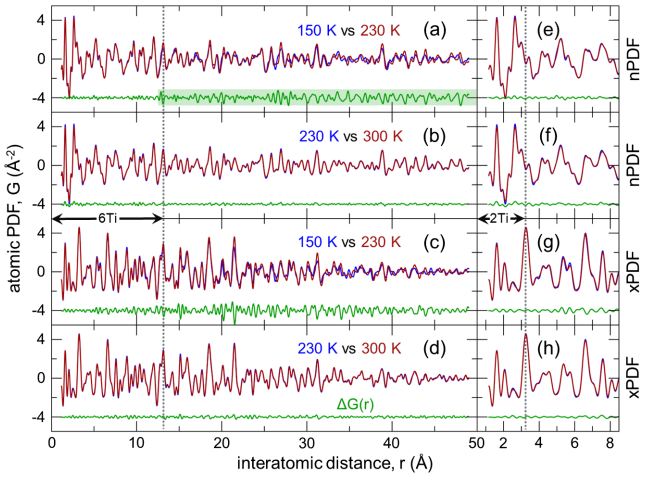

FIG. 3. Comparison of experimental PDFs. Data at temperature below (150 K) and above (230 K) the transition temperature, T_s, for neutrons (NPDF) over broad (a) and narrow (e) r ranges. Matching x-ray data (XPDF) scaled to NPDF are shown in (c) and (g). Comparison of NPDFs within the same crystallographic phase, $C2/c$, at 230 K and 300 K, is shown in (b) and (f). The same for XPDF is shown in (d) and (h). Differential PDFs, $\Delta G(r)$ are shown underneath each data, offset for clarity. The vertical dotted lines in panels (a)–(d) and (e)–(h) correspond to the fifth and the first Ti-Ti nearest neighbor distances along the zigzag chains, respectively, marked, also, by horizontal double arrows as 6 Ti (2 Ti) intrachain interatomic separations.

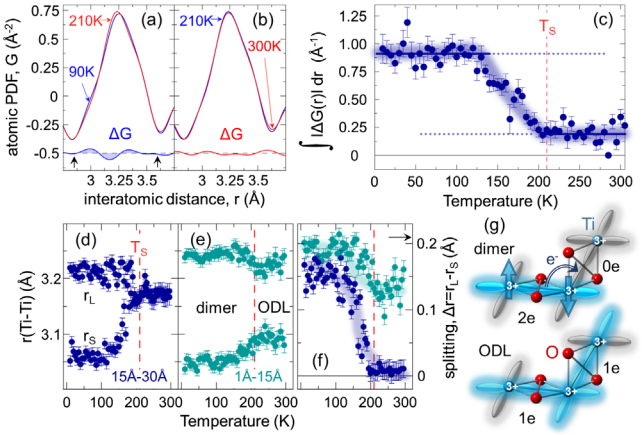

FIG. 4. The spin-singlet dimer disappearance. Comparison of XPDF data at $T_s = 210$ K with (a) 90 K and (b) 300 K data. Differentials $\Delta G = G(T) - G(T_s)$ are offset for clarity, revealing the spin-singlet signature (shaded signal) for 90 K set. (c) $\Delta G(T)$ signature (for 285 K reference) integrated over the range marked by arrows in (a) [45]. Horizontal lines are guides to the eye. The nearest neighbor Ti-Ti distances from $P\bar{1}$-based fits over (d) 15 Å $\leq r \leq$ 30 Å and (e) 1 Å $\leq r \leq$ 15 Å ranges. Corresponding r(Ti-Ti) splittings are shown in (f). (g) The spin-singlet dimer and ODL states sketched as t_{2g} orbital manifold overlaps. The color transparency indicates the bond charge filling, as noted.

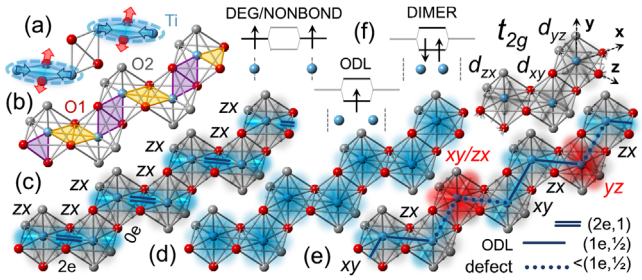

FIG. 5. $NaTiSi_2O_6$ orbital considerations. (a) TiO_2 dimerization plaquettes. (b) The two choices; the zig and the zag. (c) Dimerization of the zx variety within the $P\bar{1}$ structure. (d) Uniform chain with degenerate t_{2g} manifolds as portrayed by the $C2/c$ structure model. (e) Local model of the chain for $T \geq T_s$ featuring ODL and orbital defect states. (f) Molecular-orbital (MO) view, counterclockwise, of Ti-Ti contacts with degenerate or nonbonding Ti-Ti contacts, degeneracy-lifted MO, and dimerized Ti-Ti contacts. In the legend, DEG/NONBOND (Ti^{3+}), ODL ($1e^-$ per Ti-Ti bond), and DIMER ($2e^-$ per Ti-Ti bond). Corner insets: orbital geometry of the t_{2g} manifold (upper right), and bond chart with bond charge and bond order as noted (lower right).

integral, Fig. 4(c), is consistent with the dimers disassembling at T_s. The dimer contribution to the differential corresponds to the signal jump seen in Fig. 4(c).

To quantify this, we fit the temperature-resolved XPDF data using the low temperature $P\bar{1}$ structure over different r ranges. When the fit range excludes the local structure portion, the optimized model structure refined over 15 Å $< r <$ 30 Å range adopts two unique Ti-Ti distances below T_s, which become degenerate above T_s, Fig. 4(d), consistent with dimers vanishing. When the average structure portion of the PDF is excluded and 1 Å $< r <$ 15 Å range is used, instead, the model structure again adopts two unique Ti-Ti distances below T_s, but these two distances remain distinct above T_s, albeit with significantly reduced splitting, Fig. 4(e). Thus, at $T > T_s$ $NaTiSi_2O_6$ shows a regularization of the Ti chains over long structural length scales, but this regularization is not present locally. Residual degeneracy lifting is apparent above T_s up to 300 K [Fig. 4(f)], with splitting of 0.12(4) Å still present in our 490 K XPDF data.

Dual ODL precursor.—The behavior where short spin-singlet dimer bonds give way to longer local-symmetry-breaking transition metal contacts upon heating above the crystallographic transition is a hallmark of the ODL phenomenology seen in spinel dimer systems proximal to a localized-to-itinerant crossover. Initially observed in $CuIr_2S_4$ [27], and recently, also in $MgTi_2O_4$ [28], the ODL state is evidenced in their high temperature metallic regimes. There, at the metal-insulator transition, the spin singlet dimers comprised of pairs of strongly bonded holes ($CuIr_2S_4$) or electrons ($MgTi_2O_4$) dismount via bond charge transfer upon warming and are succeeded in the metallic phase by twice as many spatiotemporally fluctuating single charge Hund-Mulliken molecular-orbital-like states [5] that lift the t_{2g} degeneracy [27,28]. The dimer and ODL states are shown in Fig. 5(f) using energy diagram representation. The observed high crystallographic symmetry ensues from three-dimensional spatiotemporal averaging.

In addition to thermal evolution of the transition metal sublattices, the similarity of Ti pyroxenes and the spinels extends to observed pressure effects. In the spinels, pressure increases t_{2g} orbital overlaps and stabilizes the transition [59,60] and the ODL state [27]. In $LiTiSi_2O_6$, which is isostructural and isoelectronic to $NaTiSi_2O_6$, ~3.1% volume reduction also pushes T_s to higher temperature [37,45], further corroborating the equivalence of the underlying orbital behaviors. Following the spinel ODL phenomenology, in $NaTiSi_2O_6$ the Ti dimers exhibit a "$2e - 0e$"-type bond charge (ferro-orbital) order along the zigzag chains for $T < T_s$ [Fig. 5(c)], which for $T > T_s$ converts into the ODL state of antiferro-orbital character [61] with the zx-xy degeneracy lifted locally, Fig. 4(g).

However, pursuing full analogy with the spinels, particularly with $MgTi_2O_4$ which has the same Ti t_{2g} filling as in $NaTiSi_2O_6$ and whose ODL states have a two-orbital (2O-ODL) character [28] sketched in Fig. 4(g), encounters two challenges. First, in $NaTiSi_2O_6$, 2O-ODL would imply a single valued Ti-Ti distance distribution akin to the degenerate orbital case portrayed crystallographically, Fig. 5(d). This is not what is seen experimentally. Second, quasi-one-dimensional topology of Ti zigzag chains in $NaTiSi_2O_6$ necessitates a modified scenario for reconciling the different length scales.

The local bimodal distribution observed above T_s implies variation of the bond charge along the zigzag chain. We propose a model featuring short ODL bonds (bond order $1/2$) and destabilized ODL bonds (of order $< 1/2$) triggered by fluctuating orbital defects. Two such defects which interrupt the underlying antiferro-orbital order are illustrated on different chain segments in Fig. 5(e). Model considerations based on antiferro-orbital order [61] and orbital disorder [41] uncover different spin configurations very close in energy (see Fig. S8 [45]), where strong competition between the spin superexchange interaction and the Hund's-rule coupling, manifested as deviation of magnetic susceptibility from the Curie-Weiss behavior, leads to orbital frustration at high temperature [61]. Such an energy landscape may yield a mixed-orbital zx-xy defect naturally emerging as the domain wall between two antiferro-orbital ordered segments, resulting in longer Ti-Ti distances [45]. Alternatively, t_{2g} electrons on some Ti sites may populate the inert nonbonding yz orbitals, introducing the $0e$ long bonds [45]. In principle, there can be long bonds of several lengths; however, as the short ODL bonds contract, all the longer bonds mainly make rotational moves—instead of stretching—and, thus, have similar lengths, unresolvable by our analysis. The NPDF data comparison in Fig. 3(a) and

model assessment of the 290 K XPDF data [45] demonstrate that local structural correlations extend to ~13.3 Å (~6 Ti sites), implying that defect randomization beyond this length scale provides the averaging mechanism. This would lead not only to lower-energy excited states than the triplet excitations of the dimerized bonds [45], but also an increased contribution of the entropy term in the free energy at higher temperature, thus, stabilizing the ODL state in $NaTiSi_2O_6$ which can be considered to have dual (xy, xy)-(zx, zx) character indicated in Fig. 5(e) by solid blue lines connecting affected Ti sites. In this regard, the present dual ODL phenomenon can be considered as an orbital analog to the spin-crossover transition in materials with magnetic atoms changing between high- and low-spin configurations [62–64].

Concluding remarks.—Notably, a number of anomalies were observed in the $T > T_s$ regime of $NaTiSi_2O_6$ and attributed to various electronic instabilities. Anomalies include unusual temperature dependence of magnetic susceptibility [37], the lack of recovery in the muon asymmetry at longer times, and lack of sharp change in electronic relaxation rate λ at T_s in μSR measurements [65], anomalous and unusually broad phonon modes in Raman [43,58] and neutron scattering [36] and infrared reflectivity [66], glass-like temperature evolution of thermal conductivity [44], as well as anomalous peak broadening in x-ray diffraction [36]. They were assigned to short-range correlations enhancing spin-singlet dimer fluctuations [65], orbital disorder [43,58,66], rapidly fluctuating orbital occupancy [44], and presence of bond disorder due to orbital fluctuations [36], respectively. Observation of the ODL state, which is presumably dynamic, provides a concrete rationale for their understanding and invites reexamination of the transition mechanism [36,61,67]. Such high temperature anomalies could, in fact, be indicators of the ODL state in a diverse class of transition metal systems with an active orbital sector [44,68–70], reinforcing the idea of ubiquitous ODL precursors, extending the phenomenology to strongly correlated electron systems.

Work at Brookhaven National Laboratory was supported by U.S. Department of Energy, Office of Science, Office of Basic Energy Sciences (DOE-BES) under Contract No. DE-SC0012704. R. S. and H. Z. are thankful for the support from the U.S. Department of Energy under Award No. DE-SC-0020254. Neutron total scattering data were collected at the NOMAD beam line (BL-1B) at the Spallation Neutron Source, a U.S. Department of Energy Office of Science User Facility operated by the Oak Ridge National Laboratory. X-ray PDF measurements were conducted on beam line 28-ID-1 of the National Synchrotron Light Source II, a U.S. Department of Energy (DOE) Office of Science User Facility operated for the DOE Office of Science by Brookhaven National Laboratory under Contract No. DE-SC0012704.

*rkoch@bnl.gov
†Present address: Computer Science and Mathematics Division, Oak Ridge National Laboratory, Oak Ridge, Tennessee 37831, USA.
‡Present address: Institute of Physics, Chinese Academy of Science, Beijing 100190, Peoples Republic of China.
§wyin@bnl.gov
‖bozin@bnl.gov

[1] Y. Tokura, M. Kawasaki, and N. Nagaosa, Nat. Phys. **13**, 1056 (2017).
[2] Editorial, Nat. Phys. **12**, 105 (2016).
[3] B. Keimer, S. A. Kivelson, M. R. Norman, S. Uchida, and J. Zaanen, Nature (London) **518**, 179 (2015).
[4] Y. Tokura and N. Nagaosa, Science **288**, 462 (2000).
[5] S. V. Streltsov and D. I. Khomskii, Phys. Usp. **60**, 1121 (2017).
[6] M. Vojta, Rep. Prog. Phys. **81**, 064501 (2018).
[7] D. I. Khomskii, *Transition Metal Compounds* (Cambridge University Press, Cambridge, England, 2014).
[8] A. Zorko, O. Adamopoulos, M. Komelj, D. Arčon, and A. Lappas, Nat. Commun. **5**, 3222 (2014).
[9] J. K. Glasbrenner, I. I. Mazin, H. O. Jeschke, P. J. Hirschfeld, R. M. Fernandes, and R. Valenti, Nat. Phys. **11**, 953 (2015).
[10] B. H. Savitzky, I. El Baggari, A. S. Admasu, J. Kim, S.-W. Cheong, R. Hovden, and L. F. Kourkoutis, Nat. Commun. **8**, 1883 (2017).
[11] P. G. Radaelli, Y. Horibe, M. J. Gutmann, H. Ishibashi, C. H. Chen, R. M. Ibberson, Y. Koyama, Y.-S. Hor, V. Kiryukhin, and S.-W. Cheong, Nature (London) **416**, 155 (2002).
[12] A. J. Achkar, F. He, R. Sutarto, C. McMahon, M. Zwiebler, M. Hücker, G. D. Gu, R. Liang, D. A. Bonn, W. N. Hardy *et al.*, Nat. Mater. **15**, 616 (2016).
[13] N. B. Aetukuri, A. X. Gray, M. Drouard, M. Cossale, L. Gao, A. H. Reid, R. Kukreja, H. Ohldag, C. A. Jenkins, E. Arenholz *et al.*, Nat. Phys. **9**, 661 (2013).
[14] Z. Tian, Y. Kohama, T. Tomita, H. Ishizuka, T. H. Hsieh, J. J. Ishikawa, K. Kindo, L. Balents, and S. Nakatsuji, Nat. Phys. **12**, 134 (2016).
[15] T. Liang, T. H. Hsieh, J. J. Ishikawa, S. Nakatsuji, L. Fu, and N. P. Ong, Nat. Phys. **13**, 599 (2017).
[16] S. V. Borisenko, A. A. Kordyuk, A. N. Yaresko, V. B. Zabolotnyy, D. S. Inosov, R. Schuster, B. Büchner, R. Weber, R. Follath, L. Patthey *et al.*, Phys. Rev. Lett. **100**, 196402 (2008).
[17] M.-Q. Ren, S. Han, S.-Z. Wang, J.-Q. Fan, C.-L. Song, X.-C. Ma, and Q.-K. Xue, Phys. Rev. Lett. **124**, 187001 (2020).
[18] F. Wang, S. A. Kivelson, and D.-H. Lee, Nat. Phys. **11**, 959 (2015).
[19] P. O. Sprau, A. Kostin, A. Kreisel, A. E. Böhmer, V. Taufour, P. C. Canfield, S. Mukherjee, P. J. Hirschfeld, B. M. Andersen, and J. C. S. Davis, Science **357**, 75 (2017).
[20] M. D. Johannes and I. I. Mazin, Phys. Rev. B **77**, 165135 (2008).
[21] K. Terashima, Y. Sekiba, J. H. Bowen, K. Nakayama, T. Kawahara, T. Sato, P. Richard, Y.-M. Xu, L. J. Li, G. H. Cao *et al.*, Proc. Natl. Acad. Sci. U.S.A. **106**, 7330 (2009).

[22] P. A. Lee, T. M. Rice, and P. W. Anderson, Phys. Rev. Lett. **31**, 462 (1973).
[23] P. A. Bhobe, A. Kumar, M. Taguchi, R. Eguchi, M. Matsunami, Y. Takata, A. K. Nandy, P. Mahadevan, D. D. Sarma, A. Neroni *et al.*, Phys. Rev. X **5**, 041004 (2015).
[24] J. Kanamori, J. Appl. Phys. **31**, S14 (1960).
[25] H. Y. Huang, Z. Y. Chen, R.-P. Wang, F. M. F. de Groot, W. B. Wu, J. Okamoto, A. Chainani, A. Singh, Z.-Y. Li, J.-S. Zhou *et al.*, Nat. Commun. **8**, 15929 (2017).
[26] A. M. Oleś, P. Horsch, L. F. Feiner, and G. Khaliullin, Phys. Rev. Lett. **96**, 147205 (2006).
[27] E. S. Bozin, W.-G. Yin, R. J. Koch, M. Abeykoon, Y. S. Hor, H. Zheng, H. C. Lei, C. Petrovic, J. F. Mitchell, and S. J. L. Billinge, Nat. Commun. **10**, 3638 (2019).
[28] L. Yang, R. J. Koch, H. Zheng, J. F. Mitchell, W.-G. Yin, M. G. Tucker, S. J. L. Billinge, and E. S. Bozin, Phys. Rev. B **102**, 235128 (2020).
[29] D. I. Khomskii and T. Mizokawa, Phys. Rev. Lett. **94**, 156402 (2005).
[30] M. Schmidt, W. Ratcliff, P. G. Radaelli, K. Refson, N. M. Harrison, and S. W. Cheong, Phys. Rev. Lett. **92**, 056402 (2004).
[31] E. S. Božin, A. S. Masadeh, Y. S. Hor, J. F. Mitchell, and S. J. L. Billinge, Phys. Rev. Lett. **106**, 045501 (2011).
[32] R. J. Koch, T. Konstantinova, M. Abeykoon, A. Wang, C. Petrovic, Y. Zhu, E. S. Bozin, and S. J. L. Billinge, Phys. Rev. B **100**, 020501(R) (2019).
[33] H. Ohashi, T. Fujita, and T. Osawa, J. Jpn. Assoc. Mineral., Petrol. Econ. Geol. **77**, 305 (1982).
[34] D. L. Anderson, *New Theory of the Earth* (Cambridge University Press, Cambridge, England, 2012).
[35] S. V. Streltsov, O. A. Popova, and D. I. Khomskii, Phys. Rev. Lett. **96**, 249701 (2006).
[36] H. J. Silverstein, A. E. Smith, C. Mauws, D. L. Abernathy, H. Zhou, Z. Dun, J. van Lierop, and C. R. Wiebe, Phys. Rev. B **90**, 140402(R) (2014).
[37] M. Isobe, E. Ninomiya, A. N. Vasil'ev, and Y. Ueda, J. Phys. Soc. Jpn. **71**, 1423 (2002).
[38] S. V. Streltsov and D. I. Khomskii, Phys. Rev. B **77**, 064405 (2008).
[39] Z. S. Popović, Ž. V. Šljivančanin, and F. R. Vukajlović, Phys. Rev. Lett. **93**, 036401 (2004).
[40] Z. S. Popović, Ž. V. Šljivančanin, and F. R. Vukajlović, Phys. Rev. Lett. **96**, 249702 (2006).
[41] A. E. Feiguin, A. M. Tsvelik, W.-G. Yin, and E. S. Bozin, Phys. Rev. Lett. **123**, 237204 (2019).
[42] T. Egami and S. J. L. Billinge, *Underneath the Bragg Peaks: Structural Analysis of Complex Materials*, 2nd ed. (Elsevier, Amsterdam, 2012).
[43] M. J. Konstantinović, J. van den Brink, Z. V. Popović, V. V. Moshchalkov, M. Isobe, and Y. Ueda, Phys. Rev. B **69**, 020409(R) (2004).
[44] B. Rivas-Murias, H. D. Zhou, J. Rivas, and F. Rivadulla, Phys. Rev. B **83**, 165131 (2011).
[45] See Supplemental Materials at http://link.aps.org/supplemental/10.1103/PhysRevLett.126.186402 for experimental and analysis details, lengthscale estimate, pressure effect and competing states considerations, which includes Refs. [46–53].
[46] P. J. Chupas, K. W. Chapman, and P. L. Lee, J. Appl. Crystallogr. **40**, 463 (2007).
[47] A. P. Hammersley, S. O. Svenson, M. Hanfland, and D. Hauserman, High Press. Res. **14**, 235 (1996).
[48] P. Juhás, T. Davis, C. L. Farrow, and S. J. L. Billinge, J. Appl. Crystallogr. **46**, 560 (2013).
[49] J. Neuefeind, M. Feygenson, J. Carruth, R. Hoffmann, and K. K. Chipley, Nucl. Instrum. Methods Phys. Res., Sect. B **287**, 68 (2012).
[50] A. C. Larson and R. B. Von Dreele, Los Alamos National Laboratory Report No. LAUR-86-748, 2004.
[51] B. H. Toby, J. Appl. Crystallogr. **34**, 210 (2001).
[52] C. L. Farrow, P. Juhás, J. Liu, D. Bryndin, E. S. Božin, J. Bloch, T. Proffen, and S. J. L. Billinge, J. Phys. Condens. Matter **19**, 335219 (2007).
[53] P. Juhás, C. L. Farrow, X. Yang, K. R. Knox, and S. J. L. Billinge, Acta Crystallogr. Sect. A **71**, 562 (2015).
[54] M. G. Tucker, M. P. Squires, M. T. Dove, and D. A. Keen, J. Phys. Condens. Matter **13**, 403 (2001).
[55] X. Qiu, T. Proffen, J. F. Mitchell, and S. J. L. Billinge, Phys. Rev. Lett. **94**, 177203 (2005).
[56] G. J. Redhammer, H. Ohashi, and G. Roth, Acta Crystallogr. Sect. B **59**, 730 (2003).
[57] R. D. Shannon, Acta Crystallogr. A **32**, 751 (1976).
[58] M. J. Konstantinović, J. van den Brink, Z. V. Popović, V. V. Moshchalkov, M. Isobe, and Y. Ueda, J. Magn. Magn. Mater. **272–276**, E657 (2004).
[59] T. Furubayashi, T. Kosaka, J. Tang, T. Matsumoto, Y. Kato, and S. Nagata, J. Phys. Soc. Jpn. **66**, 1563 (1997).
[60] L. Ma, H. Han, W. Liu, K. Yang, Y. Zhu, C. Zhang, L. Pi, D. Liu, L. Zhang, and Y. Zhang, Dalton Trans. **46**, 6708 (2017).
[61] T. Hikihara and Y. Motome, Phys. Rev. B **70**, 214404 (2004).
[62] *Spin Crossover in Transition Metal Compounds I, II, and III. Topics in Current Chemistry*, edited by G. Gütlich and H. A. Goodwin (Springer-Verlag, Berlin, 2004), Vols. 233, 234, 235.
[63] W. Yin, arXiv:2006.08921.
[64] W. Yin, arXiv:2006.15087.
[65] P. J. Baker, S. J. Blundell, F. L. Pratt, T. Lancaster, M. L. Brooks, W. Hayes, M. Isobe, Y. Ueda, M. Hoinkis, M. Sing *et al.*, Phys. Rev. B **75**, 094404 (2007).
[66] Z. V. Popović, M. J. Konstantinović, Z. Dohčević-Mitrović, M. Isobe, and Y. Ueda, Physica (Amsterdam) **378–380B**, 1072 (2006).
[67] J. van Wezel and J. van den Brink, Europhys. Lett. **75**, 957 (2006).
[68] Z. Hiroi, Prog. Solid State Chem. **43**, 47 (2015).
[69] J. P. Attfield, APL Mater. **3**, 041510 (2015).
[70] T. Katsufuji, T. Okuda, R. Murata, T. Kanzaki, K. Takayama, and T. Kajita, J. Phys. Soc. Jpn. **85**, 013703 (2016).